AIAA 2000–2538

Acoustic Receptivity of a Blasius Boundary Layer with 2-D and Oblique Surface Waviness

Rudolph A. King
NASA Langley Research Center
Hampton, VA 23681

Kenneth S. Breuer
Brown University
Providence, RI 02912

Fluids 2000
19-22 June 2000 / Denver, CO

Acoustic Receptivity of a Blasius Boundary Layer with 2-D and Oblique Surface Waviness

Rudolph A. King*
NASA Langley Research Center
Hampton, VA 23681

Kenneth S. Breuer†
Brown University
Providence, RI 02912

An experimental investigation was conducted to examine acoustic receptivity and subsequent boundary-layer instability evolution for a Blasius boundary layer formed on a flat plate in the presence of two-dimensional (2-D) and oblique (3-D) surface waviness. The effect of the non-localized surface roughness geometry and acoustic wave amplitude on the receptivity process was explored. The surface roughness had a well defined wavenumber spectrum with fundamental wavenumber k_w. A planar downstream-traveling acoustic wave was created to temporally excite the flow near the resonance frequency of an unstable eigenmode corresponding to $k_{ts} = k_w$. The range of acoustic forcing levels, ϵ, and roughness heights, Δh, examined resulted in a linear dependence of receptivity coefficients; however, the larger values of the forcing combination $\epsilon \cdot \Delta h$ resulted in subsequent nonlinear development of the Tollmien-Schlichting (T-S) wave. This study provided the first experimental evidence of a marked increase in the receptivity coefficient with increasing obliqueness of the surface waviness in excellent agreement with theory. Detuning of the 2-D and oblique disturbances was investigated by varying the streamwise wall-roughness wavenumber α_w and measuring the T-S response. For the configuration where laminar-to-turbulent breakdown occurred, the breakdown process was found to be dominated by energy at the fundamental and harmonic frequencies, indicative of K-type breakdown.

Nomenclature

C receptivity coefficient, $u_{ts,I}/u_{ac}$.
c_{ph} phase speed of boundary-layer disturbance.
F nondimensional frequency, $2\pi f\nu/U_\infty^2$.
f frequency in Hz.
h normalized step height, $\Delta h_n/\Delta h_1$ $(n = 1, 2, 3)$.
k wavenumber, $(\alpha^2 + \beta^2)^{1/2}$.
N amplification factor, $\int_{x_l}^{x} -\alpha_i(x; f)dx$.
R Reynolds number base on δ_r, $\sqrt{U_\infty x_v/\nu}$.
Re_l Reynolds number base on length scale l, $U_\infty l/\nu$.
U mean streamwise velocity.
u rms streamwise fluctuating velocity.
x streamwise distance from model leading edge.
x_v streamwise distance from virtual origin.
y wall-normal distance from model surface.
α streamwise wavenumber.
α_i spatial amplification rate.
β spanwise wavenumber.
Δh surface roughness step height.
δ_r nondimensional length scale, x_v/R.
δ^* displacement thickness.
ϵ normalized acoustic wave amplitude, u_{ac}/U_∞.
ϕ phase of disturbance velocity.
γ coherence function.
η normalized wall-normal coordinate, $(y/x_v) \cdot R$.
λ wavelength, $2\pi/k$.
ν kinematic viscosity.
σ detuning parameter, $(\alpha_w - \alpha_{ts,I})/\alpha_{ts,I}$.
ψ wave angle.

Subscripts

ac freestream acoustic field.
I, II lower and upper branch locations.
t total disturbance component.
tr laminar-to-turbulent transition.
ts T-S wave component.
w surface roughness condition.
∞ freestream condition.

Introduction

The transition of a boundary layer from a laminar to a turbulent state plays an important role in many fluid mechanics problems since it ultimately affects basic quantities such as heat transfer and skin friction. This transition process is affected by many factors such as freestream (turbulence and/or acoustical) and surface disturbances. The process by which these disturbances are internalized to generate boundary-

*Research Engineer, Flow Physics and Control Branch.
†Associate Professor, Div. of Engineering. Member AIAA.

layer instability waves is referred to as *receptivity*.[1] A fundamental understanding of receptivity is essential since it provides the initial conditions for the subsequent growth of the unstable modes that may ultimately lead to transition. Because of the significant wavelength mismatch between the long-wavelength external disturbances and the much shorter wavelength Tollmien-Schlichting (T-S) waves, a length-scale conversion must take place to facilitate the energy transfer. It has been shown theoretically by Goldstein *et al.*,[2–4] Zavol'skii *et al.*,[5] and Ruban[6] that wavelength-reduction mechanisms can range from direct scattering associated with abrupt changes in surface conditions to the gradual wavelength reduction due to viscous boundary-layer growth.

Two general classes of receptivity regions were recognized by Goldstein, I) the leading edge regions where the boundary layer is thin and growing rapidly and II) regions further downstream where the boundary layer is forced to make a rapid adjustment. A common feature between both receptivity regions is the importance of nonparallel effects and is manifested via the disturbance motion being governed by the unsteady boundary-layer equations. Class II can be further subdivided into *localized* and *non-localized* receptivity. Localized receptivity results from an interaction between the freestream disturbances and steady localized disturbance generated by a surface inhomogeneity (e.g. humps, gaps, or suction/blowing slots). Non-localized receptivity stems from an interaction in boundary-layer flow with unsteady freestream disturbances and the steady disturbance created over surfaces with extended regions of short-scale variations (e.g. waviness, distributed roughness, uneven suction, etc.).

Choudhari[7] investigated the extent of synchronization between the surface waviness and neutral instability motion, where for perfect resonance at Branch I (lower branch) $\alpha_w = \alpha_{ts,I}$. Here α_w and α_{ts} denote the wall wavenumber and instability wavenumber, respectively and the subscript I refers to conditions at Branch I. He shows that the extent of the resonance region corresponds to a spatial extent of $\Delta x = O(x_I \cdot R_I^{-3/8})$ where x denotes streamwise distance and R Reynolds number. This implies a synchronized surface waviness will lead to instability amplitudes which are larger than those produced by an isolated surface roughness by a factor of $O(R_I^{3/8})$. Choudhari's simple analytical result helped to explain some earlier results computed by Crouch[8,9] where he found significantly larger values for non-localized receptivity versus localized receptivity. Crouch & Bertolotti[10] have shown non-localized receptivity amplitudes to be large over a wide range of surface wavenumber. They also show an increase of receptivity with surface roughness three dimensionality.

Numerous acoustic receptivity experiments have been performed with 2-D surface roughness (e.g. Aizin & Polyakov,[11] Saric *et al.*,[12–14] Zhou *et al.*,[15] Kosorygin *et al.*,[16] Breuer *et al.*,[17] Kobayashi *et al.*,[18,19] and Wiegel & Wlezien[20]). All of these studies were conducted for localized 2-D receptivity except for the study done by Wiegel & Wlezien[20] where they considered non-localized receptivity. The experiment of Zhou *et al.*[15] also considered receptivity of an oblique surface roughness. That study was conducted for localized oblique receptivity where a single strip of tape was inclined at angles up to $\psi_w = 45°$. They inferred from their measurements at a fixed streamwise location that receptivity was reduced with increased oblique angle. They did not consider the reduced linear growth rates associated with increased obliqueness.

The objectives of this research were to further understand the acoustic receptivity process for flow over wavy surfaces and to correlate theoretical results with experimental results. The approach taken was to experimentally investigate acoustic receptivity in the presence of surface waviness and the subsequent boundary-layer disturbance evolution. Previous experimental acoustic receptivity data[20] in the presence of 2-D surface waviness demonstrated excellent agreement with theoretical[7,9] receptivity coefficients. In the presence of oblique surface waviness, previous experimental data do not exist and inference made from previous experimental results[15] for a localized oblique roughness strip contradict theoretical findings. The current experimental study with 2-D waviness was conducted to (i) validate the current approach with respect to previous experimental and theoretical results and (ii) extend the measurements into regions of nonlinear T-S wave development. The measurements were then extended to include, for the first time, experimental data obtained with oblique surface waviness for comparison with theory.[10] Receptivity/stability experiments are very sensitive to the state of the mean flow and environmental disturbances. As a result, extreme care was taken to document the flow and environmental conditions to avoid ambiguous results as discussed by Nishioka & Morkovin[21] and Saric.[22]

Experimental Details

Facility and Model

The experiment was conducted in the 2 Foot by 3 Foot Low-Speed Wind Tunnel located at NASA Langley Research Center. The tunnel is a closed-loop type with a 10 : 1 contraction ratio. The test section is $0.91m$ wide by $0.61m$ high by $6.1m$ long. The turbulence-reduction devices upstream of the contraction consist of a honeycomb followed by four stainless-steel screens. Speeds of approximately $45m/s$ are attainable in the test section with measured turbulence intensities, u/U_∞, of approximately 0.1% in the range of $0.1 < f < 400Hz$. The test-section floor and ceiling are adjustable to achieve a desired streamwise pressure gradient. Two motorized traverse stages, one with

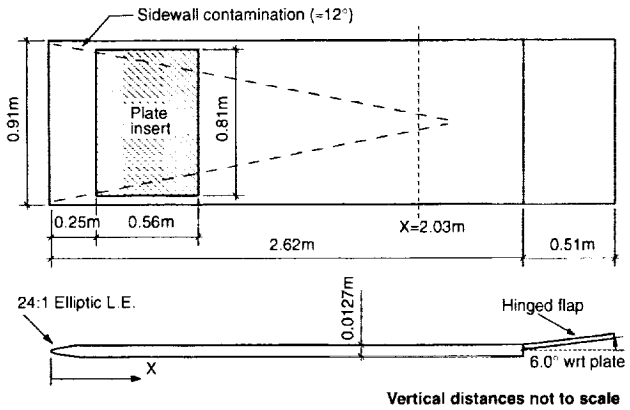

Fig. 1 Top and side views of flat plate model. The shaded region represents the location of the insert.

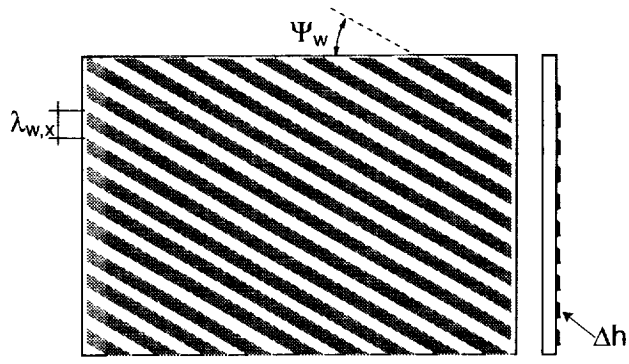

Fig. 2 Top and side views of receptivity sites investigated — $\psi_w = 0$ for 2-D and $\psi_w \neq 0$ for oblique roughness. Flow is from top to bottom.

Sample #	$\Delta h(\mu m)$	$\lambda_{w,x}(mm)$	$\psi_w(deg)$
1	17.8	50.25	0
2	35.6	50.25	0
3	71.1	50.25	0
4	35.6	58.88	0
5	35.6	53.34	0
6	35.6	50.80	0
7	35.6	49.53	0
8	35.6	48.26	0
9	35.6	45.72	0
10	35.6	50.75	15
11	35.6	52.36	30
12	35.6	55.48	45
13	35.6	56.67	32
14	35.6	54.50	31
15	35.6	50.27	29
16	35.6	48.22	28

Table 1 Table of roughness samples tested.

streamwise travel of $2.1m$ and the other with vertical travel of $150mm$, are located just above the test section ceiling. The quoted accuracies of the streamwise (x) and vertical (y) traverse stages are $\pm 166\mu m/m$ and $\pm 30\mu m/m$, respectively. A 3.8-cm streamwise slot (covered with rectangular wool felt strips to minimize air inflow/outflow) along the centerline of the tunnel ceiling is provided to accommodate a probe support for 2-D traverse motion.

The model tested was a 12.7-mm-thick flat aluminum jig plate with a 24 : 1 elliptical leading edge. A sketch of the model is shown in Figure 1. Because of the potential sensitivity of the receptivity/stability characteristics to surface roughness, the upper surface (measurement side) of the model was polished to a 0.2-μm root-mean-square (rms) surface finish. The boundary layer on the lower surface of the model was tripped using sandpaper grit to establish turbulent flow on that surface. The plate was equipped with a rectangular hole located $24.6cm$ from the model leading edge for the installation/removal of plate inserts. Five inserts were available for the test. One was used as the baseline (smooth sample) and four were used to mount various samples of receptivity sites. Further details of the experimental setup are given by King.[23]

Surface Roughness and Acoustic Excitation

Receptivity was facilitated by the use of surface waviness of height Δh and freestream acoustic excitation with amplitude u_{ac}. In previous experiments, receptivity sites were usually created by applying tape or some other adhesive material to the surface of the model. For the case of non-localized receptivity, this is a very tedious process (e.g. slight misalignment — angular and/or spatial — of the tape, Δh nonuniformities, etc.). An alternate approach for generating the surface roughness was considered, which involved the use of copper-plated circuit boards. The roughness patterns were generated using a photolithographic process where a high degree of spatial accuracy was maintained. In this process a pattern was transferred from a photomask to a material layer to produce a two-layer pattern with the roughness height Δh being equal to the copper plating thickness. The two types of patterns considered are represented in Figure 2 (the shaded areas represent copper and flow is from top to bottom). The first was a 2-D waviness pattern ($\psi_w = 0$) with the wavenumber vector parallel to the stream direction. The second was an oblique waviness pattern where the wavenumber vector makes an angle ψ_w with the stream direction. Highly localized disturbances are possible for the oblique patterns as a result of the sharp steps formed by the copper strips at the leading and trailing edges of the samples. To mitigate this effect, the copper strips were feathered down to the substrate material $6.4mm$ from both the leading and trailing edges of the samples. The roughness patterns considered are presented in Table 1.

The tunnel was equipped with an array of five 203.3-mm-diameter woofers (four flush mounted on the upstream wall and the other on the downstream wall) for acoustic excitation. The speakers were lo-

cated as described to minimize unwanted flow disturbances in the tunnel. The source of the controlled acoustic field was generated by using a dual-channel universal source and amplified with a stereo power amplifier. One channel of the source was used to drive the four upstream speakers and the second channel for the one downstream speaker. The ability to control the absolute amplitude and relative phase of the two channels made it possible to generate the required acoustic field in the test section.

Data Reduction

A single hot-wire probe was utilized to measure the streamwise velocity component that represents the bulk of the experimental data. A constant-temperature anemometer was configured to use a 1 : 20 bridge with a wire resistive overheat ratio of 1.8. A fourth-order polynomial curve fit was found to work well for the hot-wire calibration, velocity versus output voltage. Broadband and phase-locked velocity fluctuations were acquired using a typical sampling rate of $1kHz$. The mean tunnel properties (pressures, temperature and relative humidity) were measured and recorded at each data point. Estimated uncertainties of measured mean velocity, U, are in the range $\pm 1.4\%$ for $U_{max} \approx 11.1 m/s$ to $\pm 9.0\%$ for $U_{min} \approx 1 m/s$. Uncertainties of rms fluctuating velocity, u, and Reynolds number, Re, are $\pm 4.7\%$ and $\pm 4.0\%$, respectively. Details of the error analysis are given by King.[23]

Because of the type of acoustic excitation (i.e. continuous wave), the measured rms narrow-band velocities $u_l e^{i\phi_l}$ included the Stokes wave, the T-S response, and any other extraneous response (e.g. probe vibration) all at the same frequency f_o. A Stokes wave is present whenever an oscillating velocity disturbance exists in the freestream. Wlezien *et al.*[24,25] found that consistent estimates of the T-S modes are achieved when the Stokes wave was directly estimated from the measured profiles. The various decomposition approaches exploit the fact that a large mismatch in length scales exists between the Stokes and T-S waves, a 95 : 1 ratio for this study. One such approach is to make short streamwise surveys that cover approximately one T-S wavelength, λ_{ts}, at a fixed height in the boundary layer.[25,26] Over one λ_{ts}, the phase of the Stokes wave (and for that matter any probe vibration) is for all practical purposes constant. The measured response can then be plotted on the polar complex plane. Since the T-S amplitude does not vary significantly over one λ_{ts}, the centroids (Stokes wave + vibration) and the average radii (T-S amplitudes) of the off-centered spirals can be computed. The T-S wave measured here includes receptivity contributions from all possible sources, the leading edge and receptivity sites. Such surveys were obtained at wall-normal locations of lower maxima of the T-S mode shapes. Because the T-S wave is a traveling wave (i.e. linear phase ϕ_{ts} w.r.t. x), linear regression was employed to compute the streamwise T-S wavenumber, $\alpha_{ts} = |d\phi_{ts}/dx|$, which was used to obtain wave kinematic results (e.g. $\lambda_{ts,x} = 2\pi/\alpha_{ts}$, $c_{ph} = 2\pi f_o/\alpha_{ts}$, etc.).

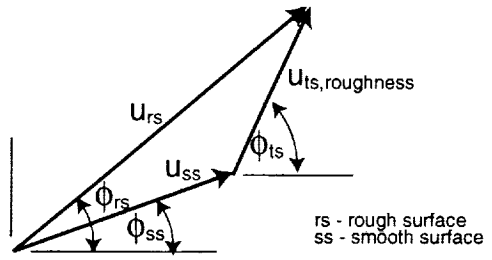

Fig. 3 Graphical representation of decomposition method used for wall-normal surveys.

Most of the disturbance measurements were acquired by making wall-normal surveys, complete and partial boundary-layer profiles, at selected x locations. The approach taken here to extract the T-S wave component is a slight variation from earlier methods.[25,26] Two sets of wall-normal disturbance profiles were obtained at the same x locations and with the same acoustic forcing levels. One set was taken with the smooth surface (denoted with "ss" subscripts) and the second with a rough surface (denoted by subscript "rs"). The disturbance measurements obtained on the smooth surface include components of the Stokes wave, T-S wave due to leading-edge receptivity, and extraneous disturbances. The disturbances acquired with receptivity sites include the same components measured on the smooth surface in addition to the T-S wave component due to the controlled roughness. This is shown graphically in Figure 3. The T-S wave component due to roughness was obtained using the following

$$u_{ts} e^{i\phi_{ts}} = u_{rs} e^{i\phi_{rs}} - u_{ss} e^{i\phi_{ss}}. \qquad (1)$$

Here the T-S component includes receptivity due to acoustic scattering at the roughness sites of (1) the freestream acoustic field and (2) the leading-edge generated T-S wave. The receptivity due to the scattering of the leading-edge generated T-S wave was assumed negligibly small. This was supported by leading-edge receptivity measurements in the present study and a previous experiment[24] for a 24 : 1 elliptic leading edge, both of which indicated small T-S responses.

Linear stability results presented here were computed using a computer code by Malik[27] that incorporates quasi-parallel spatial stability theory. These results were used to facilitate the computation of the receptivity coefficients, C $(= u_{ts,I}/u_{ac})$, referenced to the Branch I location. Here $u_{ts,I}$ denotes the maximum rms T-S amplitude at Branch I and u_{ac} the rms freestream acoustic velocity fluctuation. Measurements of u_{ts} were made downstream of Branch I to take advantage of the linear amplification re-

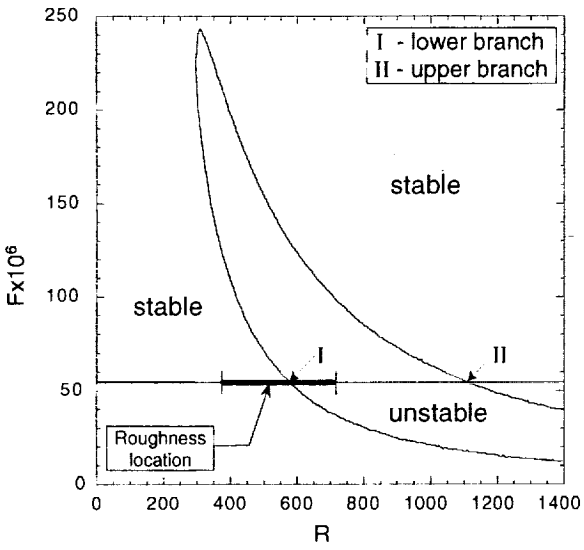

Fig. 4 Neutral stability curve for a Blasius boundary layer with 2-D disturbances.

gion for improved signal-to-noise ratios. The values of $u_{ts,I}$ were obtained by applying linear stability theory (LST) to the measured values of u_{ts} such that

$$C = u_{ts}\epsilon^{-N}/u_{ac} \tag{2}$$

where N is the amplification factor obtained from LST.

Experimental Approach

This experiment was conducted with a nominal freestream velocity of $U_\infty = 11.1m/s$ and temperature of $21°C$. A nominally zero-streamwise-pressure-gradient boundary layer was obtained for flow over a flat plate (Blasius flow). A planar downstream-traveling acoustic wave was used to temporally excite the flow with frequency f_o. A simple approach was employed to generate the wave train by conducting two streamwise surveys in the freestream above the model, each at the same spatial coordinates. One survey was taken with only the upstream set of speakers activated and the second survey with only the downstream speaker energized. Applying the method of superposition, the combined wave field with both sets of speakers active was simulated. A scale factor and phase shift were selected to give the desired response, namely, a constant rms amplitude distribution.

The dimensionless frequency of the T-S wave for all cases was $F = 55 \times 10^{-6}$, which translates to physical acoustic forcing frequency of $f_o = 71Hz$. Figure 4 shows a plot of a neutral stability curve for a Blasius boundary layer with 2-D disturbances. A line representing the experimental frequency along with the roughness location and extent ($\Delta x = 0.56m$) is shown in the figure. Note that the location of the surface waviness was selected such that its midpoint was near the location of Branch I to maximize the receptivity. The wavenumber of the surface roughness, k_w, was selected such that it matched the T-S wavenumber, k_{ts}, at Branch I to provide a near-resonance condition. Three roughness heights, Δh, and three acoustic forcing levels, ϵ ($= u_{ac}/U_\infty$), were examined for the 2-D waviness. The matrix configuration used to combine Δh and ϵ are given in Table 2. Detuning was examined for the 2-D and oblique roughness patterns. This was achieved by maintaining the same forcing frequency, f_o, and varying the streamwise wall roughness wavenumber, α_w, while the spanwise wavenumber, β_w, remained unchanged.

	Δh_1	$\Delta h_2 = 2\Delta h_1$	$\Delta h_3 = 4\Delta h_1$
ϵ_1	$\epsilon_1\Delta h_1$	$2\epsilon_1\Delta h_1$	$4\epsilon_1\Delta h_1$
$\epsilon_2 \doteq 2\epsilon_1$	$2\epsilon_1\Delta h_1$	$4\epsilon_1\Delta h_1$	$8\epsilon_1\Delta h_1$
$\epsilon_3 \doteq 4\epsilon_1$	$4\epsilon_1\Delta h_1$	$8\epsilon_1\Delta h_1$	$16\epsilon_1\Delta h_1$

Table 2 Roughness heights and forcing levels examined — $\Delta h_1 = 17.8\mu m$, $\epsilon_1 = 7.6\times10^{-5}$ ($SPL = 84.8$).

Results and Discussion

Base Flow Measurements

Mean Flow

Normalized streamwise velocity measurements just outside the boundary layer, $y \approx 25.4mm$, revealed a pressure recovery region near the leading edge of the model with deviations of less than 0.25% of U_∞ from Branch I location to the end of the survey region ($0.5 < x < 2.03m$). The velocities along the plate insert location for roughness placement ($24.6 < x < 80.8cm$) were all within 1% of U_∞. For the properly configured model, the boundary layer developed into a nominally zero-pressure-gradient boundary layer downstream of the recovery region. For proper comparisons with theory, a virtual origin was defined and streamwise locations referenced to this origin are denoted by x_v. The virtual origin was computed by first acquiring detailed boundary-layer velocity profiles on the smooth (baseline) model every $254mm$ starting at $x = 508mm$. A linear-regression curve fit was applied to the square of the measured displacement thickness (δ^*) versus x. The curve fit was used to extrapolate upstream to $\delta^* = 0$ and the corresponding x value was used as the virtual origin, $x = 65.8mm$.

A more stringent characterization of the flow was to the compute the shape factor H for each profile. The values of the experimental shape factors were $H = 2.60 \pm 1.5\%$ in excellent agreement with the theoretical Blasius value of $H = 2.59$. A plot of the measured normalize velocity profiles and the theoretical Blasius profile versus the normalized wall-normal coordinate η is presented in Figure 5. Excellent agreement between the profiles is evident. The two dimensionality of the mean flow outside the sidewall contamination region (see Figure 1) was validated by obtaining boundary-layer measurements at various spanwise locations.

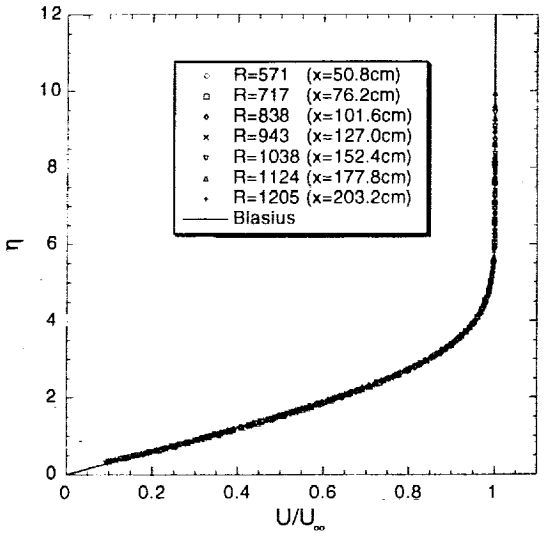

Fig. 5 Normalized velocity profiles at selected streamwise locations.

Freestream Characteristics

Freestream turbulent intensity measurements $(u/U)_\infty$, where u is the broadband rms value of velocity fluctuations ($0.1 < f < 400Hz$), were obtained using a single hot-wire probe. Values of $(u/U)_\infty \approx 0.1\%$ were measured over the entire streamwise survey region. More important than the magnitude of $(u/U)_\infty$, the power spectral density of the fluctuating velocity, PSD_u, provided relevant information on the frequency content of the disturbance environment. Measured PSD_u's indicate a $-5/3$ power law ($PSD_u \propto f^{-5/3}$), supporting the hypothesis that the freestream disturbances were composed predominantly of decaying turbulence. Most of the freestream energy were contained at very low frequencies, below $1Hz$. More than 90% of the broadband energy was contained between $0.1Hz$ and $1Hz$ illustrating the importance of specifying frequency bandwidths when quoting turbulent levels. Limited dynamic pressure measurements were obtained from four pressure transducers flush mounted on the test section sidewalls.[23] Correlations of the dynamic pressure signals confirm the absence of coherent disturbances in the freestream environment near the designed forcing frequency, f_o, of the experiment that can distort the interpretation of the results.

As a final flow-quality check, the transition Reynolds number, Re_{tr}, was measured on the smooth plate. This was done by placing the hot-wire probe at a fixed location in the boundary layer and slowly sweeping through the tunnel speed range. An average value of $Re_{tr} = 3.2 \times 10^6$ was measured, indicating low freestream turbulent levels and a smooth model surface (for comparison, refer to data of Re_{tr} versus freestream turbulence cited in White,[28] pp. 433-436). For a configuration with 2-D waviness ($\Delta h = 71.1\mu m$) and $\epsilon = 0$, a 25% reduction in Re_{tr} was observed.

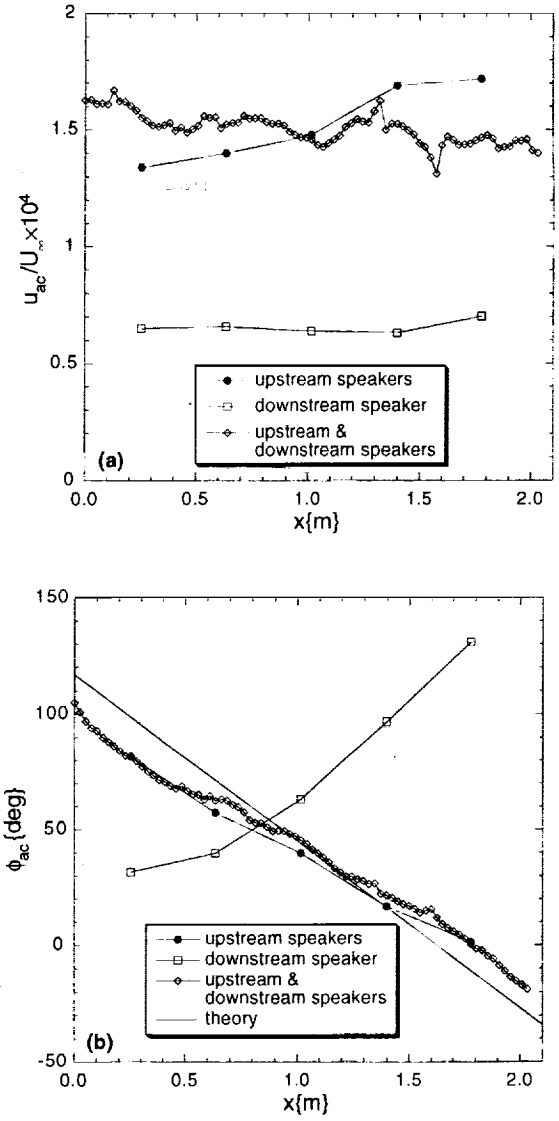

Fig. 6 Measured freestream acoustic field generated in the test section above the model surface — (a) amplitude and (b) phase streamwise distributions.

Acoustic-Field Characterization

Measurements of the controlled freestream acoustic field are shown in Figure 6 in the form of (a) amplitude and (b) phase streamwise distributions. Data with only the upstream speakers and only the downstream speaker activated are also presented for completeness in the figure. In the vicinity of the insert region ($24.6 < x < 80.8cm$), the variation of the acoustic amplitude was small. The phase distribution in part (b) of the figure indicates a predominantly downstream-traveling wave. Values of the acoustic rms amplitudes, u_{ac}, used for normalization in subsequent sections are the average values measured over the plate insert. Streamwise measurements taken at various wall-normal and spanwise locations verified the planar structure of the acoustic field.

$\psi_{ts}\{\text{deg}\}$	R_I	$\lambda_{ts,I,x}\{mm\}$
0	585	50.2
15	583	50.8
30	578	52.4
45	574	55.5

Table 3 Tabulated data of Reynolds numbers and streamwise T-S wavelength at Branch I for disturbance wave angle ψ_{ts} obtained from LST. Note that $R \approx 85.92 \cdot x_v^{1/2}$ where x_v is in centimeters.

Receptivity Measurements

Effect of ϵ, Δh, and ψ_w on Receptivity

The influences of acoustic forcing level, ϵ, roughness height, Δh, and roughness obliqueness, ψ_w, were examined by conducting measurements with the matrix arrangement shown in Table 2 and utilizing samples $1-3$ and $10-12$ of Table 1. At the location of Branch I (see Table 3), the largest roughness height, Δh_3, normalized by δ^* was 0.05 and the corresponding roughness Reynolds number was $Re_{\Delta h_3} = 47$. Therefore, all roughness heights considered were well within the roughness Reynolds number range of a *hydraulically smooth* surface (see White,[28] pp. 436-439). Measurements were obtained over a range of Reynolds numbers, $R > 570$ ($x > 50.8cm$), that extended beyond the location of Branch II. The results to be presented here were obtained for the condition where the wavelength of the wall roughness λ_w matched that of the T-S wave at Branch I, the *near-resonance* condition. In this context, the term near-resonance describes the condition when $\alpha_w = \alpha_{ts,I}$ which does not account for the finite speed of the freestream acoustic wave, i.e. $\alpha_{ac} \neq 0$.

Measurements of T-S amplitudes at locations just downstream of Branch I indicated a virtually linear response of u_{ts} with both u_{ac} and Δh in the presence of 2-D roughness. T-S amplitude eigenfunctions are shown in Figure 7 at $R = 1038$ for various forcing products, $\epsilon \cdot \Delta h$. The rms T-S amplitude, u_{ts}, was normalized by u_{ac} and h where h is the step height normalized by the smallest step height. The linear behavior is evident from the data collapse in the figure and indicates linear receptivity for all acoustic and wall forcing levels considered. The 180° phase shift at $\eta \approx 2\delta^*$ is evident in the plots of the T-S phase ϕ_{ts} (not shown). Measured data depicting the streamwise evolution of the T-S eigenfunctions indicate good agreement with LST for locations upstream of where nonlinear effects first became apparent in the near-wall region. The nonlinear effects became evident at the same x location for a given value of $\epsilon \cdot \Delta h$, independent of the individual values of ϵ or Δh. More on the nonlinear evolution of the T-S instability is discussed later.

To investigate the influence of T-S wave obliqueness on receptivity, samples 2 and $10-12$ (refer to

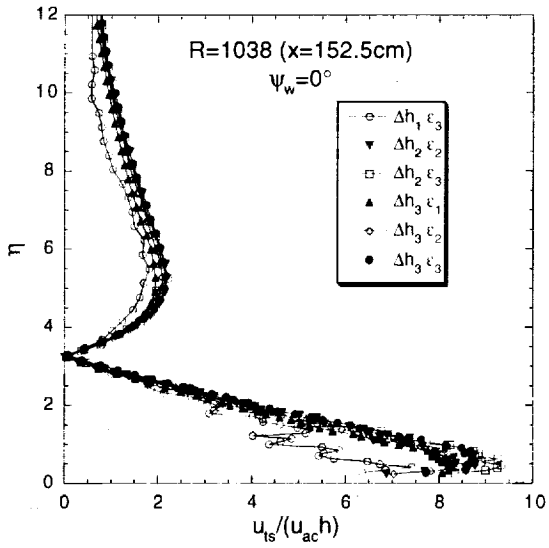

Fig. 7 Normalized T-S amplitude profiles with 2-D surface waviness for various values of ϵ and Δh.

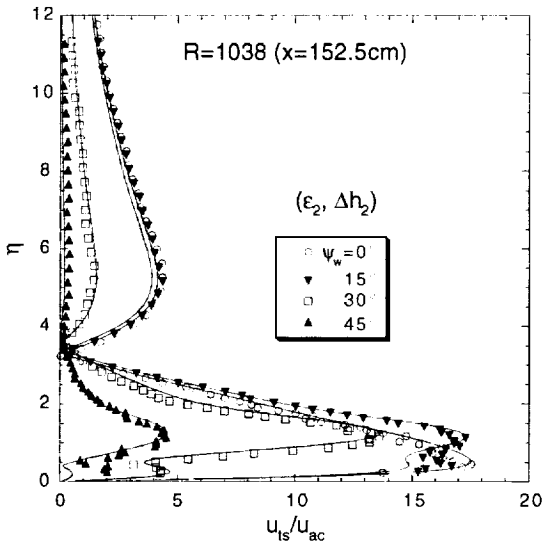

Fig. 8 T-S amplitude profiles for various values of ψ_w at $R = 1038$.

Table 1) were used to generate the oblique T-S waves by the application of oblique waviness. The roughness wavenumbers were selected to create a near-resonance condition at Branch I for each ψ_w considered (see Table 3 for tabulated values of the streamwise T-S wavelength at Branch I, $\lambda_{ts,I,x}$ ($= 2\pi/\alpha_{ts,I}$)). Measured and LST T-S amplitudes at $R = 1038$ ($x = 152.4cm$) are presented in Figure 8 for various ψ_w. The LST results were normalized to match the experimental amplitudes at the maximum of u_{ts} for these profiles. Note that the relative peak (inner and outer) amplitudes of the measured T-S profiles do not scale directly with LST results. This may be due in part to nonparallel effects not accounted for in LST since nonparallelism becomes more important for three-dimensional disturbances (see Bertolotti[29]). Nevertheless, the salient

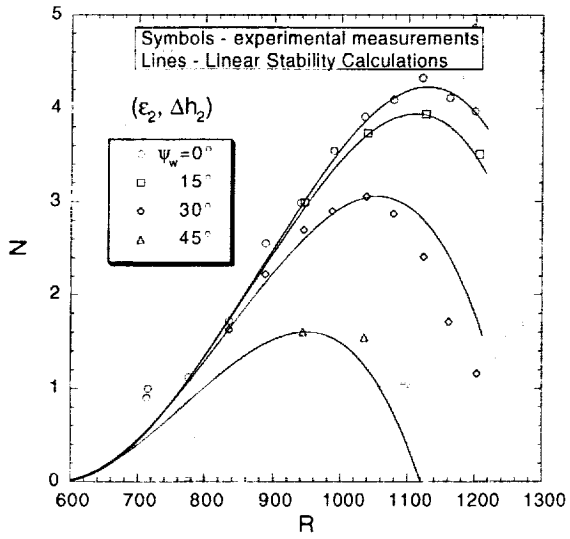

Fig. 9 Streamwise amplification data for various values of ψ_w.

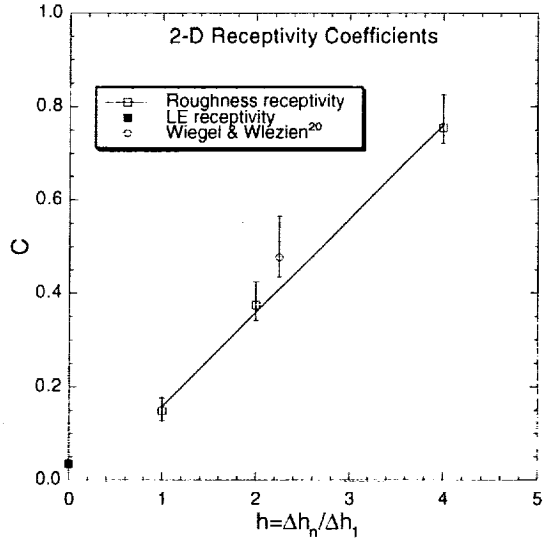

Fig. 10 Non-localized 2-D receptivity coefficients from present experiment ($F = 55 \times 10^{-6}$) and past experiment ($F \approx 46 \times 10^{-6}$) as a function of Δh.

features of the eigenfunction profiles were captured by LST. For 2-D disturbances, a single peak in the near-wall region below the critical layer ($\eta \approx 1$) was evident. As the disturbances became oblique, some residual of this peak remained and the appearance of a dual peak structure in the near-wall region — which straddles the critical layer — is evident. An upward shift of the global maximum to a wall-normal location above the critical layer was observed. The amplitude of the apparent residual peak reduced with increased obliqueness. An upward shift of the wall-normal location of the 180° phase jump was also evident.

The streamwise amplitude distribution of the measured T-S eigenfunctions were compared to the amplification predicted by LST. Figure 9 shows a plot of N-factor from LST versus Reynolds number along with the experimentally measured maximum T-S amplitudes. The experimental amplitudes ($\ln(u_{ts}/u_{ac})$) were obtained from measured eigenfunction profiles taken at selected x locations and scaled for comparison with LST. Excellent agreement between the measured and LST data for 2-D waviness is evident except for the large values of u_{ts} measured for $R = 717$ just downstream of Branch I (in a region over the wavy surface). The large values of u_{ts} measured in the near-wall region just downstream of Branch I may partly be explained by the non-monotonic increase of the total instability response resulting from the localized peak (overshoot) in the receptivity region due to the external forcing.[7,9] The location of Branch II is in excellent agreement with LST. The data also demonstrate (not shown) that consistent amplification curves are obtainable by tracking either the inner or outer peaks, provided the response is linear. Excellent agreement was also observed between the measured and LST amplification curves for small oblique angles. The agreement became less attractive for the larger oblique angles, particularly near the location of Branch II. Again, this may be a result of nonparallel effects not captured by LST. Agreement between the measured and experimental amplifications is important since theory (e.g. LST) is required to backtrack the effective Branch I amplitudes in an accurate fashion.

The receptivity coefficients, C, to be presented were referenced to Branch I and computed utilizing Equation 2. The stipulation that all values of u_{ts} employed were obtained downstream of Branch I and the roughness surface and upstream of Branch II was implemented. Figure 10 shows a plot of the experimental 2-D receptivity coefficients (plus linear regression fit) versus the normalized step height. Data from the experiment of Wiegel & Wlezien[20] for a different nondimensional frequency ($F \approx 46 \times 10^{-6}$) are also included. The symbols represent mean values and the error bars the maximum plus/minus deviations observed in the measurements for all values of ϵ. The leading-edge receptivity coefficient for the smooth surface ($h = 0$) was calculated using data obtained in short streamwise surveys. The small values of the leading-edge receptivity coefficients ($C \approx 0.035$) support the decomposition assumption discussed previously. Good agreement is observed between the present and previous[20] experimental receptivity coefficients. The corresponding T-S wave kinematics were inferred from data obtained with short streamwise surveys (i.e. ϕ_{ts} versus x data) where α_{ts} ($= -d\phi_{ts}/dx$) was computed directly. The average T-S wave phase speed, $\bar{c}_{ph}/U_\infty = 0.33$ ($c_{ph} = 2\pi f_o/\alpha_{ts}$), at $R = 1038$ for all values of ϵ and Δh considered is in excellent agreement with LST result, $c_{ph}/U_\infty = 0.33$.

Figure 11 shows a plot of measured receptivity coefficients as a function of ψ_w along with theoretical

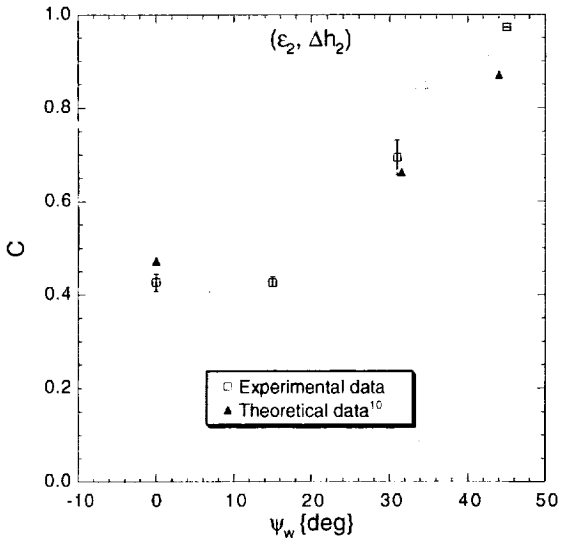

Fig. 11 Measured ($F = 55 \times 10^{-6}$) and theoretical ($F = 56 \times 10^{-6}$) receptivity coefficients versus ψ_w.

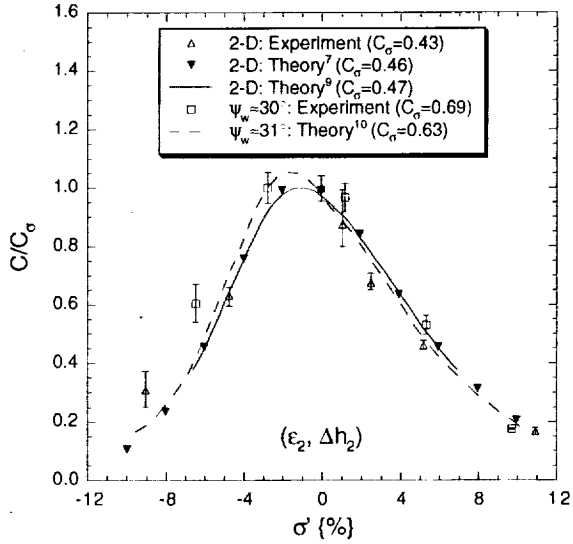

Fig. 12 Measured ($F = 55 \times 10^{-6}$) and theoretical ($F = 55 \times 10^{-6}$ and $F = 56 \times 10^{-6}$) receptivity coefficients versus the detuning parameter.

data ($F = 56 \times 10^{-6}$) by Crouch & Bertolotti.[10] The agreement between the measured and theoretical data is good, thereby providing experimental evidence of increased receptivity with increased wave obliqueness. The confidence level for the value of the experimental receptivity coefficient at $\psi_w = 45°$ is not very high since only one data point was used to obtain the value of C. This may be one explanation for the large difference observed there along with the fact that the mode-interaction theory used to compute the theoretical values of C degrades with three-dimensionality, which is largely attributable to nonparallel effects.[10] The overall agreement between the measured and LST c_{ph}/U_∞ with respect to ψ_w is good, within the experimental uncertainty of the measurements.

Effect of detuning on Receptivity

In this section, results are presented for the so-called *detuned* conditions. Detuning is referred to as the condition when there is a mismatch between the wavelengths of the wall roughness and the T-S mode ($\lambda_w \neq \lambda_{ts}$) for a given disturbance frequency. The energy transfer from the forced disturbance becomes less efficient as the degree of detuning is increased. As a measure of the detuning, the detuning parameter σ is defined as

$$\sigma = \frac{\alpha_w - \alpha_{ts,I}}{\alpha_{ts,I}}. \qquad (3)$$

In previous studies (e.g. Wiegel & Wlezien[20]), detuning was generally examined by varying U_∞, which consequently varied $\alpha_{ts,I}$. This was done because of difficulties realized in varying α_w. Because of the type of receptivity sites used in the current study, σ was varied by changing α_w. Detuning data for both 2-D and oblique waviness were obtained using samples 2 and 4 – 9 and samples 11 and 13 – 16, respectively (refer to Table 1). All the data were obtained with the forcing product $\epsilon_2 \cdot \Delta h_2$.

The maximum receptivity was not expected at the near-resonance condition $\alpha_w = \alpha_{ts,I}$ as predicted by receptivity theory that assumes incompressible flow (infinite acoustic wave speed). To account for a finite acoustic wave speed, one has to take into consideration the wavenumber of the freestream acoustic wave, α_{ac}, as conjectured by Wiegel & Wlezien.[20] For the present experiment, care was taken to acoustically excite the freestream with a downstream-traveling wave. Choudhari & Streett[30] discussed the finite wave speed effect and showed that a resonance condition exists when $(\alpha_w, \beta_w) = (\alpha_{ts,I} - \alpha_{ac}, \beta_{ts,I})$ since $\beta_{ac} = 0$ here.

Measured and theoretical[7,9,10] receptivity coefficients are presented in Figure 12 for various values of the detuning parameter (modified) σ'. The roughness height used to compute the theoretical receptivity coefficients[7,9,10] for single-mode waviness was the first Fourier coefficient of a square wave pattern with height Δh, namely the mode corresponding to the fundamental wavenumber, α_w, with amplitude $\Delta h/\pi$. The parameter σ' shifts the values of σ in Equation 3 to account for the finite acoustic wave speed. The detuning parameters are related by $\sigma' = \sigma + \alpha_{ac}/\alpha_{ts,I}$ where the respective values of $\alpha_{ac}/\alpha_{ts,I}$ for the 2-D and oblique waviness are 1.04% and 1.08%. The receptivity coefficients are normalized by C_σ where C_σ is the maximum value of C (measured or computed) except for the theoretical C_σ value for the oblique roughness which is the theoretical value of C at the same σ' (≈ -2.8) as the corresponding experimental value. Good agreement is obtained between the measured and theoretical values demonstrating the effectiveness of non-localized receptivity over a wide range of α_w. A maximum difference of less than 10% was obtained between the measured maximum and the corresponding theoretical value of

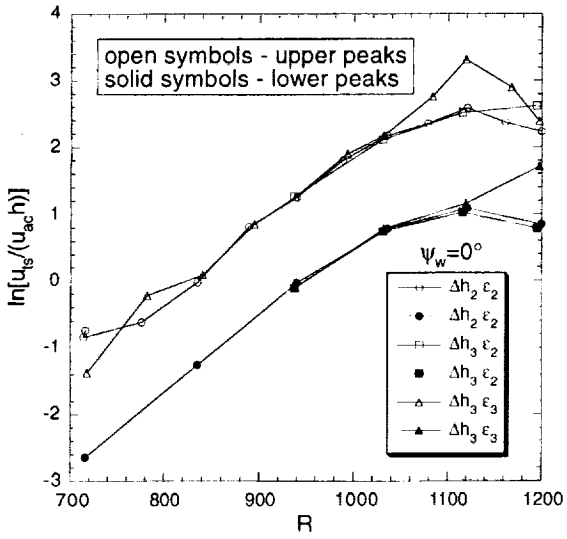

Fig. 13 Streamwise amplification data with 2-D disturbances for various values of $\epsilon \cdot \Delta h$.

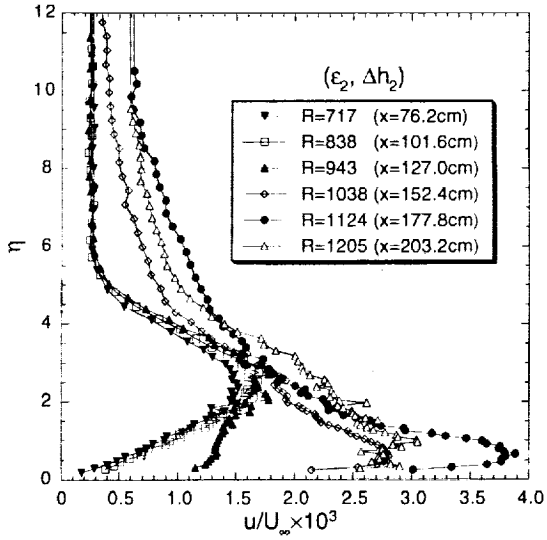

Fig. 14 Measured broadband rms fluctuating velocity for forcing combination of $\epsilon_2 \cdot \Delta h_2$.

the receptivity coefficients, C_σ.

Disturbance Evolution

In this section, data describing the evolution of the boundary-layer disturbance field are presented. Emphasis is placed on results obtained in the presence of 2-D surface roughness since nonlinear behavior was evident only for large values of the forcing combination ($\epsilon \cdot \Delta h$). The broadband results obtained with oblique waviness were qualitatively similar to those obtained with 2-D waviness and intermediate forcing, $\epsilon_2 \cdot \Delta h_2$. For this reason, oblique results are not discussed explicitly in this section except where minor differences were noted. The measured streamwise amplitude distribution of the normalized T-S eigenfunctions were compared for various values of $\epsilon \cdot \Delta h$ in Figure 13. The solid symbols represent data of the outer peak and the open symbols data of the inner (maximum) peak. Nonlinear effects are evident from the amplification curves for the forcing products of $\epsilon_2 \cdot \Delta h_3$ and $\epsilon_3 \cdot \Delta h_3$ (see for comparison Figure 9). For the case of $\epsilon_2 \cdot \Delta h_3$, nonlinear effects are apparent only in the near-wall region and first become discernible when $u_{ts}/U_\infty > 0.8\%$ at $R \approx 1120$ (just upstream of Branch II, $R_{II} = 1129$). For the largest forcing product ($\epsilon_3 \cdot \Delta h_3$), nonlinearity is evident in both the near-wall and outer regions of the boundary layer. The nonlinearity was observed first near the surface and eventually spread throughout the shear layer due to the interaction of normal vorticity, which is driven by the mean shear (see Cohen, Breuer, & Haritonidis[31]). Nonlinearity was first observed for $u_{ts}/U_\infty > 1.0\%$ at $R \approx 1034$ ($R < R_{II}$).

Broadband ($2 < f < 400Hz$) rms fluctuating velocities, u, measured for $\epsilon_2 \cdot \Delta h_2$ are presented in Figure 14. For this intermediate forcing level, the flow remained laminar (see Figure 13). In the early stages ($R < 943$, $x < 127cm$), the rms velocity profiles resemble those of Klebanoff modes as measured by Klebanoff,[32] and Kendall.[33,34] The profiles are indistinguishable from profiles measured on the smooth model surface with no controlled acoustic forcing (baseline configuration) — $\epsilon = 0$, $\Delta h = 0$. The maximum rms fluctuations occur near the midpoint of the boundary-layer thickness ($\eta \sim 2.3$). The rate of increase of the maximum rms velocity at each streamwise station is small for these low-freestream turbulent intensity levels. For measurements taken further downstream ($R > 943$), the contributions from the T-S wave become dominant in the near-wall region and near the boundary-layer edge due to the dual-lobe shape of the T-S eigenfunctions. Near the midpoint of the boundary layer, the rms velocities are still consistent with those measured on the baseline configuration. As shown using parabolized stability theory by Herbert and Lin,[35] the T-S waves and these low-frequency Klebanoff modes appear to exist independently, but both may contribute to the intensity at a given frequency. For $\epsilon_3 \cdot \Delta h_3$ where nonlinear effects and consequent breakdown occurred, increases of one to two orders of magnitude in the maximum values of u were observed. Power spectral densities of the fluctuating streamwise velocity, PSD_u, corresponding to data presented in Figure 14 are shown in Figure 15. The spectra are shown for data obtained at $\eta \approx 2.3$. The controlled acoustic forcing is clearly evident in the spectra at $f_o = 71Hz$. The spectra shown consist of significant low-frequency energy, a characteristic of Klebanoff modes. Modest amplification at frequencies ($f < 20Hz$) below the unstable T-S modes is evident at $R = 1205$ ($x = 203.2cm$) and was also observed for the baseline configuration. As expected, significantly more amplification is evident in the unstable T-S band.

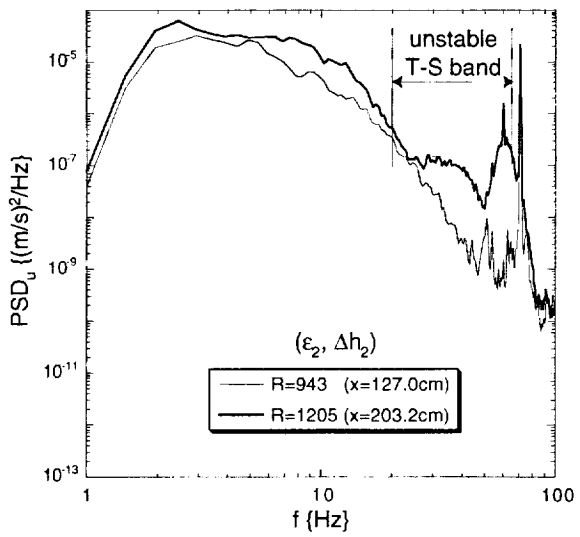

Fig. 15 Spectra of fluctuating velocity near $\eta \approx 2.3$ for forcing product of $\epsilon_2 \cdot \Delta h_2$.

To investigate the coherent nature of the boundary-layer disturbance field, particular consideration was given to disturbances at the fundamental (f_o), subharmonic ($f_o/2$), and first harmonic ($2f_o$) frequencies. The coherence function, γ, (between the designated instability wave and the input signal used for the acoustic forcing) at the three frequencies of interest was computed. Significant values of γ for $\epsilon_2 \cdot \Delta h_2$ were obtained at the fundamental and harmonic frequencies for a wall-normal location corresponding to the maximum of the T-S wave amplitude; however, negligible coherence was observed for the subharmonic band. The amplification curves at the selected frequencies reveal that the harmonic disturbance essentially mirrors the amplification of the fundamental disturbance. As a result, the harmonic disturbance was believed to be merely driven by the fundamental and a result of a nonlinear self-interaction. No amplification was observed at the subharmonic frequency. Coherence and amplification data for $\epsilon_3 \cdot \Delta h_3$ are shown in Figure 16. A sharp roll off in coherence of the fundamental and harmonic disturbances are evident for $R > 1038$ ($x > 152.4cm$) indicating the onset of significantly nonlinear behavior leading to turbulence. This is in agreement with results inferred from the amplification curves in Figure 13. Again, negligible coherence was observed at the subharmonic frequency. Referring to part (b) of the figure, it is evident from the amplification curves that the harmonic disturbance grew at rate different from that of fundamental, indicating a strong nonlinear interaction at the harmonic frequency. The growth seen at the subharmonic frequency was not due to phase-locked amplification, but a result of broadening of the spectra indicative of the breakdown process. The transition Reynolds number for this scenario was $Re_{tr} \approx 1.2 \times 10^6$ which is approximately one-third of the baseline Re_{tr} ($\approx 3.2 \times 10^6$).

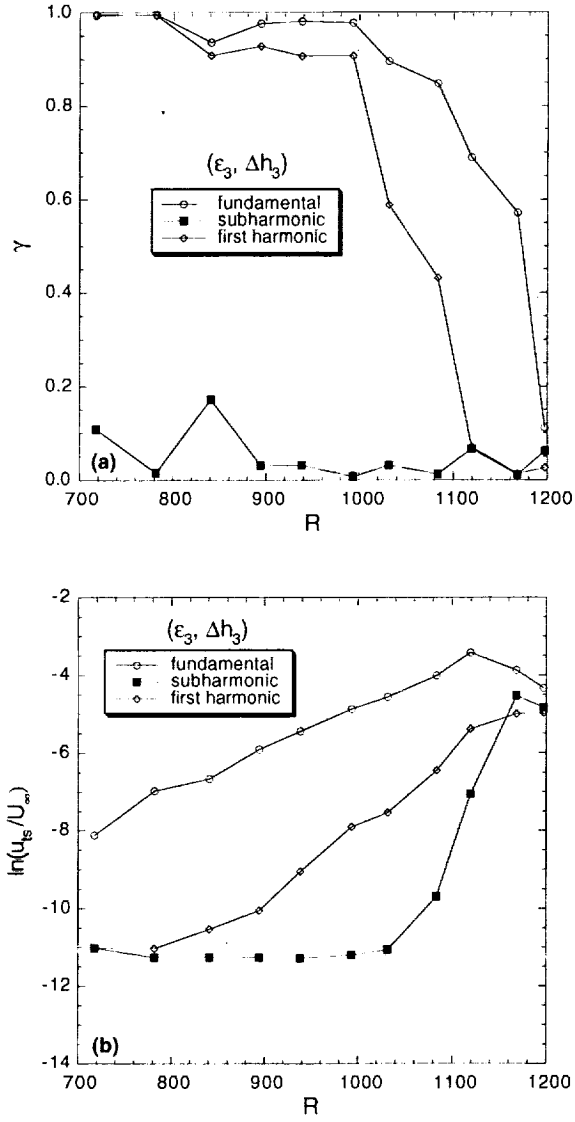

Fig. 16 Data showing the fundamental, subharmonic, and first harmonic (a) coherence functions and (b) growth curves for $\epsilon_3 \cdot \Delta h_3$.

Finally, broadband spectra for the intermediate and largest forcing levels are presented in Figure 17 for a range of streamwise locations ($717 < R < 1205$ or $76.2 < x < 203.2cm$) at wall-normal locations corresponding to the maximum of u_{ts}. For the intermediate forcing level ($\epsilon_2 \cdot \Delta h_2$) in part (a) of the figure, the energy and associated growth at the fundamental forcing frequency ($f_o = 71Hz$) and its first harmonic are clearly evident. The energy at $f = 120Hz$ is associated with electronic noise as evident from the constant streamwise amplitude. Amplification of broadband energy centered about $f \approx 60Hz$ presumably a result of the *natural* tunnel disturbance environment is discernible in the spectra for $x > 127.0cm$ ($R > 943$). Broadband amplification is also evident about $f \approx 130Hz$ for $x > 152.4cm$ ($R > 1038$). This latter broadband energy is possibly an interaction between

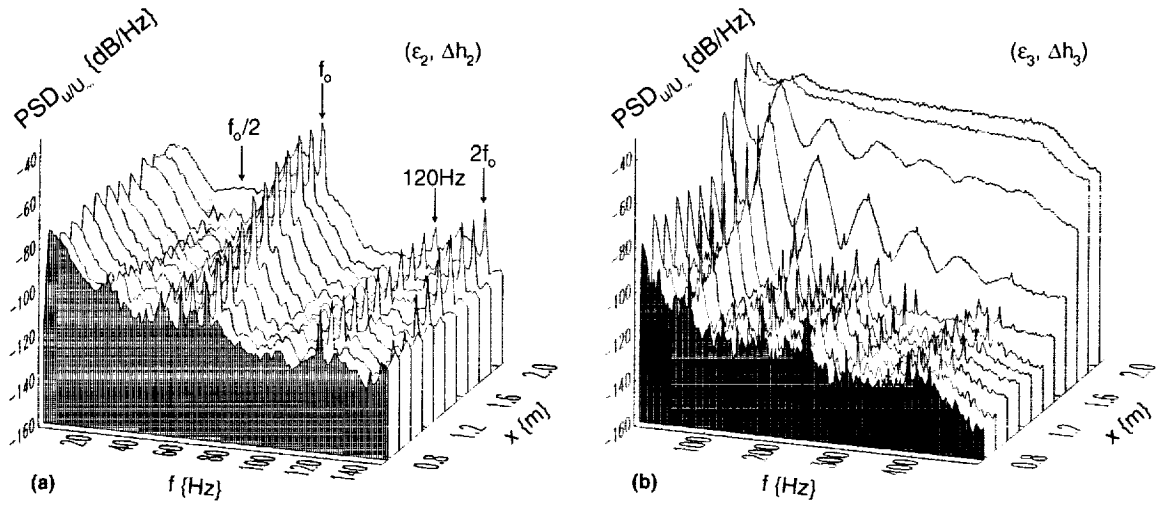

Fig. 17 Spectra of streamwise velocity taken at $u_{ts,max}$ over a range of streamwise locations for (a) $\epsilon_2 \cdot \Delta h_2$ and (b) $\epsilon_3 \cdot \Delta h_3$. The subharmonic, fundamental, and first harmonic frequencies (along with 120-Hz electronic noise) are denoted in part (a) of the figure.

the forced T-S wave and the naturally occurring broadband T-S field. The broadband amplification about $f \approx 130Hz$ was not evident for the oblique waviness configuration ($\psi_w = 30°$). This is believed to be due to the reduced energy amplitudes of both the forced T-S wave and the naturally occurring broadband T-S field. The situation was quite different for the largest forcing combination in part (b) of the figure. The presence of significant energy at the fundamental and higher harmonic frequencies is clearly discernible at the onset of nonlinearity ($x > 152.4cm$ or $R > 1038$). The harmonic bands broaden until a developed turbulent spectrum was obtained. Broadband amplification in the unstable T-S band of frequencies as seen for the intermediate forcing level above was not discernible in the present spectra. Similar harmonic-dominated spectra were obtained in the experiment of Breuer *et al.*[17] This type of breakdown from laminar to turbulent flow is indicative of a K-type breakdown as obtained by the classical results of Klebanoff *et al.*[36,37] The selectivity of the single-frequency wave, imposed by the controlled acoustic forcing and receptivity sites, created a dominant primary T-S wave with amplitudes much larger than other two- and three-dimensional modes resulting from background disturbances. The primary mode at the fundamental frequency dominated the breakdown process and resulting nonlinear interactions produced harmonics as is evident in the disturbance spectral evolution (see Figure 17(b)).

Concluding Remarks

The most widely used transition prediction tool is currently the e^N method, which is a semiempirical method based on linear amplification (not disturbance amplitudes) of unstable modes. This approach does not include any physics regarding the role of the external disturbance environment on the boundary-layer instability development. Improved transition prediction tools based on an amplitude approach need to incorporate physics relating the effects of the environment on the transition process. This approach needs, as an input, information about the initial boundary-layer disturbance amplitude, and this need is met by a better understanding of the receptivity process. Consequently, receptivity plays a crucial role in any transition prediction tool that utilizes an amplitude based approach. The objective of the current research was to better understand the acoustic receptivity process and subsequent disturbance evolution in the presence of wavy surfaces and correlate results with theory. Experimental investigations were conducted to examine acoustic receptivity and subsequent boundary-layer instability evolution in the presence of 2-D and oblique surface waviness. These investigations provided a data base which can ultimately be used to validate current and future theoretical receptivity/transition models needed to improve the current understanding of laminar-to-turbulent transition.

A subtle accomplishment of the current study was the ability to introduce a variety of steady boundary-layer disturbances via the well-defined receptivity sites without any measurable first-order effects on the base flow. This study explored, in addition to 2-D acoustic receptivity, the subsequent evolution of the boundary-layer instability. The current acoustic receptivity measurements with 2-D waviness are in excellent agreement with the existing experimental measurements[20] and theoretical results.[7,9] For a configuration where laminar-to-turbulent breakdown occurred ($\epsilon_3 \cdot \Delta h_3$), the breakdown process was found to be dominated by energy at the fundamental and higher-harmonic frequencies, indicative of K-type breakdown. Receptivity data were acquired experimentally for the first time

over oblique wavy surfaces ($\psi_w = 15°, 30°$, and $45°$) to measure the dependence of receptivity on roughness obliqueness (or three dimensionality). The current findings were in substantial agreement with theory and experimentally confirmed the earlier theoretical results[10] that receptivity increases markedly with wave obliqueness. Boundary-layer transition was not observed for the forcing combination ($\epsilon_2 \cdot \Delta h_2$) used with the oblique surface waviness.

The transition Reynolds number measured on the baseline configuration was $Re_{tr} \approx 3.2 \times 10^6$. The value of Re_{tr} for the 2-D surface roughness with a forcing combination of $\epsilon_3 \cdot \Delta h_3$ was significantly less ($\sim 60\%$ reduction) than that for the baseline configuration. The drastic shifts in the value of Re_{tr} demonstrate the sensitivity of the transition location to the freestream environment and surface conditions.

References

[1]Morkovin, M. V., "Critical evaluation of transition from laminar to turbulent shear layers with emphasis on hypersonically traveling bodies," Technical Report AFFDL-TR-68-149, Wright-Patterson Air Force Base, 1969.

[2]Goldstein, M. E., "The evolution of Tollmien-Schlichting waves near a leading edge," *J. Fluid Mech.*, Vol. 127, 1983, pp. 59–81.

[3]Goldstein, M. E., Sockol, P. M., and Sanz, J., "The evolution of Tollmien-Schlichting waves near a leading edge Part 2. Numerical determination of amplitudes," *J. Fluid Mech.*, Vol. 129, 1983, pp. 443–453.

[4]Goldstein, M. E., "Scattering of acoustic waves into Tollmien-Schlichting waves by small streamwise variations in surface geometry," *J. Fluid Mech.*, Vol. 154, 1985, pp. 509–529.

[5]Zavol'skii, N. A., Reutov, V. P., and Rybushkina, G. V., "Excitation of Tollmien-Schlichting waves by acoustic and vortex disturbance scattering in boundary layer on a wavy surface," *J. Appl. Mech. Tech. Phys.*, Vol. 25, 1984, pp. 355–361, (English translation, 1983).

[6]Ruban, A. I., "On the generation on Tollmien-Schlichting waves by sound," *Fluid Dynamics*, Vol. 19, 1985, pp. 709–716.

[7]Choudhari, M., "Boundary-layer receptivity due to distributed surface imperfections of a deterministic or random nature," *Theoret. Comput. Fluid Dynamics*, Vol. 4, 1993, pp. 101–117.

[8]Crouch, J. D., "Initiation of boundary-layer disturbances by nonlinear mode interactions," *Boundary Layer Stability and Transition to Turbulence*, edited by D. C. Reda, H. L. Reed, and R. Kobayashi, Vol. 114, ASME, 1991, pp. 63–68.

[9]Crouch, J. D., "Non-localized receptivity of boundary layers," *J. Fluid Mech.*, Vol. 244, 1992, pp. 567–581.

[10]Crouch, J. D. and Bertolotti, F. P., "Nonlocalized receptivity of boundary layers to three-dimensional disturbances," AIAA Paper 92-0740, 1992.

[11]Aizin, L. B. and Polyakov, N. F., "Acoustic generation of Tollmien-Schlichting waves over local unevenness of surface immersed in streams," *Preprint 17, Akad. Nauk USSR, Siberian Div., Inst. Theor. Appl. Mech., Novorsibirsk*, 1979, (in Russian).

[12]Saric, W. S., Hoos, J. A., and Radeztsky, R. H., "Boundary-layer receptivity of sound with roughness," *Boundary Layer Stability and Transition to Turbulence*, edited by D. C. Reda, H. L. Reed, and R. Kobayashi, Vol. 114, ASME, 1991, pp. 17–22.

[13]Saric, W. S., Hoos, J. A., and Kohama, Y., "Boundary-layer receptivity: Part 1. Freestream sound and 2D roughness strips," CEAS-CR-R-90191. College of Engineering and Applied Sciences Report, Arizona State University, 1990.

[14]Saric, W. S. and White, E. B., "Influence of high-amplitude noise on boundary-layer transition to turbulence," AIAA Paper 98-2645, 1998.

[15]Zhou, M. D., Liu, D. P., and Blackwelder, R. F., "An experimental study of receptivity of acoustic waves in laminar boundary layers," *Experiments in Fluids*, Vol. 17, 1994, pp. 1–9.

[16]Kosorygin, V. S., Radeztsky, R. H., and Saric, W. S., "Laminar boundary-layer, sound receptivity and control," *Laminar-Turbulent Transition*, edited by R. Kobayashi, Springer-Verlag, 1995, pp. 517–524.

[17]Breuer, K. S., Dzenitis, E. G., Gunnarsson, J., and Ullmar, M., "Linear and nonlinear evolution of boundary layer instabilities generated by acoustic-receptivity mechanisms," *Phys. Fluids*, Vol. 8, 1996, pp. 1415–1423.

[18]Kobayashi, R., Fukunishi, Y., Nishikawa, T., and Kato, T., "The receptivity of flat-plate boundary-layers with two-dimensional roughness elements to freestream sound and its control," *Laminar-Turbulent Transition*, edited by R. Kobayashi, Springer-Verlag, 1995, pp. 507–514.

[19]Kobayashi, R., Fukunishi, Y., and Kato, T., "Laminar flow control of boundary layers utilizing acoustic receptivity," *Sixth Asian Congress of Fluid Mechanics*, Vol. 1, 1996, pp. 629–632.

[20]Wiegel, M. and Wlezien, R. W., "Acoustic Receptivity of laminar boundary layers over wavy walls," AIAA Paper 93-3280, 1993.

[21]Nishioka, M. and Morkovin, M. V., "Boundary-layer receptivity to unsteady pressure gradients: experiments and overview," *J. Fluid Mech.*, Vol. 171, 1986, pp. 219–261.

[22]Saric, W. S., "Low-speed boundary-layer transition experiments," *Transition: Experiments, Theory & Computations*, edited by T. C. Corke, G. Erlebacher, and M. Y. Hussaini, Oxford, 1994, pp. 1–114.

[23]King, R. A., *Receptivity and growth of two- and three-dimensional disturbances in a Blasius boundary layer*, Ph.D. thesis, Massachusetts Institute of Technology, Cambridge, MA, February 2000.

[24]Wlezien, R. W., Parekh, D. E., and Island, T. C., "Measurement of acoustic receptivity at leading edges and porous strips," *Appl. Mech. Rev.*, Vol. 43, No. 5, 1990, pp. S167–S174.

[25]Wlezien, R. W., "Measurement of acoustic receptivity," AIAA Paper 94-2221, 1994.

[26]Saric, W. S., Wie, W., Rasmussen, B. K., and Krutckoff, T. K., "Experiments on leading-edge receptivity to sound," AIAA Paper 95-2253, 1995.

[27]Malik, M. R., "e^{Malik}: A new spatial stability analysis program for transition prediction using the e^N method," High Technology Report No. HTC-9203, Hampton, Virginia, 1992.

[28]White, F. M., *Viscous Fluid Flow*, McGraw-Hill, Inc, New York, New York, 1974.

[29]Bertolotti, F. P., *Linear and nonlinear stability of boundary layers with streamwise varying properties*, Ph.D. thesis, The Ohio State University, Columbus, OH, 1991.

[30]Choudhari, M. and Streett, C. L., "Theoretical prediction of boundary-layer receptivity," AIAA 94-2223, 1994.

[31]Cohen, J., Breuer, K. S., and Haritonidis, J. H., "On the evolution of a wave packet in a laminar boundary layer," *J. Fluid Mech.*, Vol. 225, 1991, pp. 575–606.

[32]Klebanoff, P. S., "Effect of freestream turbulence on the laminar boundary layer," *Bull. Amer. Phys. Soc.*, Vol. 10, No. 11, 1971, pp. 1323.

[33]Kendall, J. M., "Experimental study of disturbances produced in a pre-transitional laminar boundary layer by weak freestream turbulence," AIAA Paper 85-1695, 1985.

[34]Kendall, J. M., "Boundary layer receptivity to freestream turbulence," AIAA Paper 90-1504, 1990.

[35]Herbert, T. and Lin, N., "Studies of boundary-layer receptivity with Parabolized Stability Equations," AIAA Paper 93-3053, 1993.

[36]Klebanoff, P. S. and Tidstrom, K. D., "Evolution of amplified waves leading to transition in a boundary layer with zero pressure," NASA TN D-195, 1959.

[37]Klebanoff, P. S., Tidstrom, K. D., and Sargent, L. M., "The three-dimensional nature of boundary-layer instability," *J. Fluid Mech.*, Vol. 12, 1962, pp. 1–34.